RSC Advances

ROYAL SOCIETY OF CHEMISTRY

www.rsc.org/advances

Flexible Pd/CeO_2-TiO_2 nanofibrous membrane with high efficient ultrafine particulate filtration and improved CO catalytic oxidation performance†

Wei Li, Yan Wang, Botao Ji, Xiuling Jiao* and Dairong Chen*

Abstract

Flexible CeO_2-TiO_2 fibrous membrane was prepared by electrospinning combined sol-gel method. The composition, structure and morphology of the membrane were thoroughly investigated with XRD, FT-IR, N_2 adsorption-desorption, SEM and TEM. The tensile-strength of the TiO_2-CeO_2 was evaluated by tensile tester and the highest strength (1.38 MPa) was attained at the Ce and Ti molar ratio of 5:100, which was 3 times as high as that of pure TiO_2. After Pd was loaded on the fibers, the strength of fibrous membrane (1.28 MPa) stayed almost the same. Moreover, the Pd/CeO_2-TiO_2 fibrous membrane exhibits high thermal stability against long time usage and retains the strength up to 1.22 MPa after 400 °C for 20 h. Such a prior strength performance is mainly due to the effective size control of the particles composed the nanofibers, which endows the fibrous membrane with the application potential in the high efficiency particle filtration. The best filtration performance was the efficiency of 99.86% and corresponding pressure drop of 178 Pa. At the same time, the fibrous membrane also exhibits good low-temperature CO oxidation performance with a complete conversion of CO to CO_2 at 200 °C and no decrease of catalytic activity over 30 h. The excellent properties of Pd/CeO_2-TiO_2 fibrous membrane enrich the application of inorganic fibrous membrane in the air filtration and catalysis simultaneously.

1. Introduction

With the development of economy and urbanization, more and more waste gas was released, which brought about

School of Chemistry & Chemical Engineering, National Engineering Research Center for Colloidal Materials, Shandong University, Jinan 250100, P. R. China. Email: cdr@sdu.edu.cn, jiaoxl@sdu.edu.cn.

† Electronic supplementary information (ESI) available: XRD patterns and FT-IR spectra of the xerogel fibrous membrane and those calcined at 500 °C; FE-SEM images of TiO_2, TC01, TC05, and TC10; N_2 adsorption-desorption isotherms and pore size distribution curves; X-ray energy dispersive spectrometry (EDS) and corresponding elemental mapping of TC05; TEM image, SEM images, XRD patterns and optical image of Pd/TC05, XPS spectrum of Pd in the Pd/TC05 nanofibers. See DOI: 10.1039/b000000x/.

serious air pollution. It is announced that the outdoor air pollution is one of the main causes of cancer death by the International Agency for Research on Cancer (IARC) of the World Health Organization (WHO).[1] Like the heavy smog in China, the air pollution has drawn much attention of the public.[2] The vehicle exhaust and industrial waste gas are the two major sources of air pollution due to the incomplete combustion existing widely in the energy conversion process of fossile fuels,[3,4] which simultaneously contain inhalable particles and poisonous components such as CO, NO and etc.[5,6] The fine inhalable particulate matter (with aerodynamic diameter less than 2.5 μm, PM2.5) is a serious danger to human health. It is estimated that 2.1 million deaths are related with cardiopulmonary diseases and lung cancer caused by PM2.5 every year. CO is one of the most common pollutions in air, which can do a lot of harm to the nervous and cardiovascular systems.[7] Therefore, the treatment of waste gas is an effective route to solve the air pollution.

At present, a two-step treatment is employed to deal with air pollution, namely the filtration of the dust and the elimination of poisonous gases.[8] However, there are obvious disadvantages in the processes such as poor recyclability of catalysts and heat consumption in the filtration. Therefore, seeking a filter media against high temperature with ability to remove toxic gases is a great challenge and benefits to solve the existed problems.

Fibrous membrane was one of the most widely used filter media for its high dust-holding capacity, high specific surface area and excellent filtration performance.[9] The "slip effect" will reduce the pressure drop with the diameters of the fibers decreasing.[10,11] Electrospinning technique attracts great interests in preparing nanofibers owing to its convenience and effectiveness.[12-14] To date, many ploymer fibrous membranes have been fabricated *via* electrospinning and show wide application prospect in the field of air filtration.[15-17] However, most of them cannot sustain the temperature higher than 250 °C, which prevents them from being used as a high-temperature filter media. As to inorganic nanofibers, many flexible membranes have been studied in the separation process under severe conditions.[18-20] Recently, flexible SiO_2 and γ-Al_2O_3 fibrous membranes have been reported and

showed high-efficiency as filter media for fine particles at high temperature.[21,22] Hence, it is feasible to endow the inorganic fibrous filter media with the catalytic activity.

The noble metal catalysts are usually used for catalyzing oxidation of CO.[23] It is one of the most direct, simple, cheap and effective ways to eliminate CO at low temperature. When the transition metal oxides, such as TiO_2,[24] CeO_2,[25] MnO_2,[26] and so on,[27-29] were adopted as the supports, the catalytic activity of the composite is highly improved comparing to pure catalyst. In this view, Pd/TiO_2 catalyst is one of potential candidates. The redox and surface properties of TiO_2 are influenced by particle sizes, phase modifications and structural defects, especially the combination of other easily variable valency metal oxides. Recently, there have been great interests in using ceria as a promoter of titania since it was suggested to improve the thermal stability and redox properties of TiO_2.[30] When the noble metal is supported on CeO_2-TiO_2 composite, the support could also participate in the reaction *via* the involvement of lattice oxygen.[30-32] The strong metal-support interaction in Pd/CeO_2-TiO_2 favors the reduction of both PdO and CeO_2, which contributes to the high activity of CO oxidation at low temperature.[33] Besides, the grain sizes of the TiO_2 can be adjusted by embedding CeO_2 into TiO_2 matrix.[34]

Many fibrous catalysts of CO oxidation have been prepared *via* electrospinning and exhibited high activity due to their high specific area and the uniform distribution of active ingredient.[35,36] Although many CeO_2-TiO_2 fibrous membranes have been prepared in the same way,[37-39] the brittleness and low strength make them hardly be handled and utilized in practice. It is also not mentioned to apply the CeO_2-TiO_2 membranes in the fields of high efficiency air filter and CO oxidation. To the best of our knowledge, self-standing flexible CeO_2-TiO_2 fibrous membrane has not been reported.

Herein, the flexible Pd/CeO_2-TiO_2 fibrous membrane is successfully prepared *via* the careful control of the sol-gel process and the calcination procedure for the first time. The strength of the membranes closely relies on the contents of ceria. The high strength of the membranes makes them strong enough to be used as the air filter

media. Besides, by loading Pd on CeO_2-TiO_2 supports, the catalytic performance for CO oxidation is largely improved. So, the flexible inorganic fibrous membrane, Pd/CeO_2-TiO_2, not only exhibits good performance in air filtration, but also in the catalytic oxidation of CO.

2. Experimental section

2.1. Chemicals

All the chemicals were purchased commercially and used without any further purification. The starting materials included polyethylene oxide (PEO, Mw≈500,000), tetrabutyl titanate (TBT, analytical grade), cerium(III) nitrate hexahydrate ($Ce(NO_3)_3 \cdot 6H_2O$, analytical grade), hydrochloric acid (HCl, 36-38%, analytical grade), palladium chloride ($PdCl_2$, analytical grade), methanol (CH_3OH, analytical grade) and deionized water with a resistance of 18.2 MΩ.

2.2. Synthesis

Synthesis of CeO_2-TiO_2 fibrous membrane

In a typical preparation, 3.40 g of TBT and certain amount of $Ce(NO_3)_3 \cdot 6H_2O$ were dissolved into 5.0 mL of methanol. 0.25 mL of concentrated HCl (10 M) was added into the solution. This solution transformed to a transparent sol after being vigorously stirred for 1 h, followed by the addition of 0.035 g of PEO at 60 °C to adjust the viscosity. The obtained sol was cooled down to room temperature, and then transferred into a hypodermic syringe. The sol was then electrospun into fibrous membrane with the applied voltage of 20.0 kV and the distance between the syringe and collector of 20 cm. The flow rate of the precursor sol was 1 mL/h and the humidity was maintained around 20% RH. The as-prepared gel fibrous membranes were collected and dried at 70 °C for 24 h. The membrane was firstly calcined at 400 °C for 2 h with a heating rate of 1.0 °C/min; and then the temperature was raised to 500 °C (2.0 °C/min) for 2 h. After being cooled down in the furnace, the CeO_2-TiO_2 fibrous membrane was obtained, which were labeled as TC01, TC05 and TC10 with the molar ratio of TiO_2:CeO_2 =100:1,

20:1 and 10:1 respectively.

Synthesis of Pd/CeO_2-TiO_2 fibrous membrane

The synthesis process of Pd/CeO_2-TiO_2 fibrous membrane was the same as the CeO_2-TiO_2 fibrous membrane except the concentrated HCl solution (10 M) of $PdCl_2$ (0.25 M) was used instead of the concentrated HCl solution. The content of loaded Pd is 0.5 wt% in the Pd/CeO_2-TiO_2 fibrous membrane. As a reference, the Pd–TC05 was obtained by impregnating the TC05 nanofibers with $PdCl_2$ solution, followed by drying and calcinations, in which the Pd content was same as that in the Pd/TC05 fibrous membrane.

2.3. Characterization

The morphology and microstructure of the membranes were characterized by a transmission electron microscope (TEM, JEOL-1010) with an accelerating voltage of 100 kV, a high resolution TEM (HR-TEM, JEOL-2100) with an accelerating voltage of 200 kV and field emission-scanning electron microscope (FE-SEM JEM-6700F). X-ray energy dispersive spectrometry (EDS) and corresponding elemental mapping were obtained in the JEM-6700F FE-SEM. X-ray diffraction (XRD) patterns were collected on a Rigaku D/Max 2200PC diffractometer with a graphite monochrometer and CuKα radiation (λ=0.15418 nm). Fourier transform infrared (FT-IR) spectra were recorded on a Nicolet 5DX FT-IR spectrometer using KBr pellet method. The mechanical properties were measured on a tensile tester (XG-1A, Shanghai New Fiber Instrument Co., Ltd., China) with a clamp distance of 5 mm and a drawing speed of 1.0 mm/min. N_2 adsorption-desorption isotherms were measured on a QuadraSorb SI apparatus at 77 K and before the measurement the samples were degassed under vacuum at 100 °C for 12 h. The surface area (S_{BET}) was calculated using the Brunauer-Emmett-Teller (BET) method and the pore size distribution was derived from the desorption branch using the Barrett-Joyner-Halenda (BJH) theory. X-ray photoelectron spectra (XPS) were recorded on a Perkin-Elmer PHI-5300 ESCA spectrometer with a 35.75 eV pass energy and an AlKα line excitation source. The core levels were calibrated according to the C 1s binding energy (BE) of

284.6 eV.

2.4. Air filtration test

The filtration performance of the membrane was detected on a TSI model 8130 automated filter tester (TSI, Inc., MN, USA)，which could deliver charge neutralized NaCl aerosols with a mass median diameter of 300-500 nm, and the continuous air-flow rate was 32 L min^{-1} or 5.3 cm s^{-1} of face velocity at room temperature.

2.5. CO catalytic oxidation test

Catalytic oxidation of CO was carried out in a quartz tubular flow microreactor with an internal diameter of 6.0 mm at atmospheric pressure. For each test, 50.0 mg of the sample was directly placed at the center of the reactor using quartz glass wool as plugs without any pretreatment. The reaction stream consisted of 1.0% CO and 10.0% O_2 (by volume) balanced with N_2. The weight hourly space velocity (WHSV) of the stream was 72,000 mL g^{-1} h^{-1}. After the reaction stream entered the reactor at room temperature, the test for CO oxidation was conducted at a heating rate of 2.0 °C min^{-1} from room temperature to 400 °C or until CO was completely converted into CO_2. The start temperature for the complete conversion of CO was used to evaluate the activity of the sample. The produced CO_2 and unreacted CO were periodically analyzed online with a gas chromatograph (Shimadzu GC-2010) equipped with a column packed with carbon molecular sieves, a post-column methanator and a flame ionization detector.

3. Results and discussion

3.1. Structure and composition of flexible CeO_2-TiO_2 membranes

To obtain the flexible fibrous membrane, it is important to control the hydrolysis and condensation of the titania sol. The addition of concentrated HCl solution can prevent tetrabutyl titanate from being excessively hydrolyzed and gelation. PEO was dissolved after the HCl solution was added due to the poor solubility of PEO in methanol. The mixture was heated to 60 °C to form a uniform sol. During the electrospinning process, the sol was charged

and stretched under the electronic field force, and the xerogel fibrous membrane could be formed on the collector. The temperature and humidity should be well controlled to remove the solvent quickly. The thickness of the membranes could be adjusted by changing the spinning time.

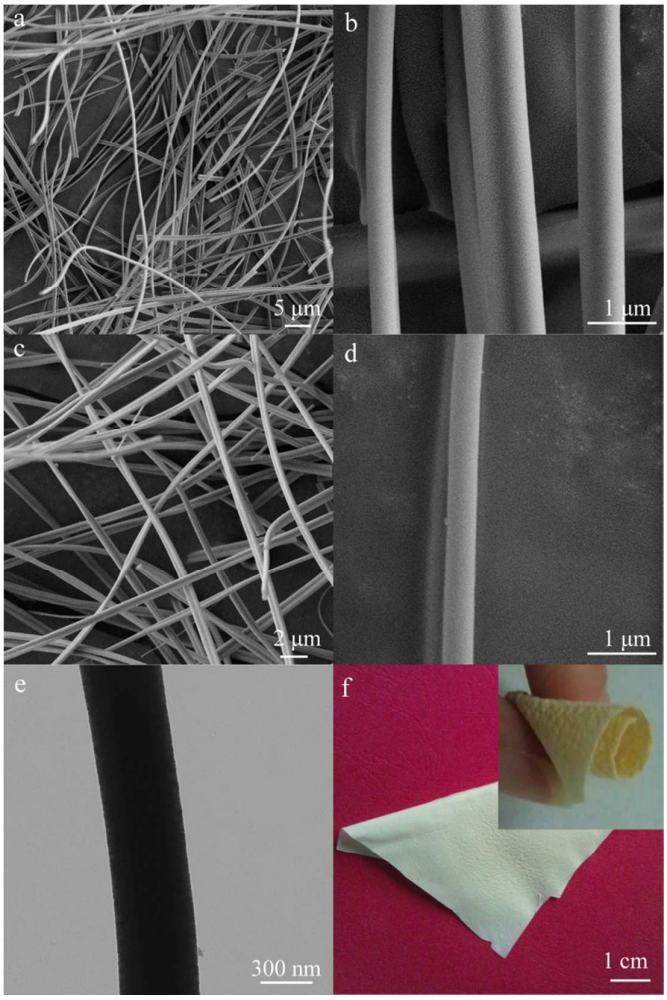

Fig. 1 SEM images of xerogel fibers (a, b) and TC05 sample (c, d), TEM image (e) and optical images (f) of TC05 sample.

The morphology and microstructures of the CeO_2-TiO_2 fibrous membranes were thoroughly studied by SEM and TEM. As shown in Fig. 1a and b, the xerogel fibers have a high aspect ratio of more than 1,000 with an average diameter of ca.850 nm. The surface of the fibers was smooth and no obvious defects were observed. The shape is slightly tabular, which could be attributed to the quick evaporation of solvents during the electrospinning

process. After being calcined at 500 °C, the size of xerogel fibrous membrane shrank nearly 50%, but still remained its integrated membrane form. The fibers still retained high aspect ratio and smooth surface (Fig. 1c). With the decomposition of organic components and the densification during the calcinations, the average diameter of fibers decreased to 350 nm (Fig. 1d). From the TEM image of TC05, the dense structure of the fibers can be obtained and observable cracks and pores can hardly be found. After bending many times (Fig. 1f), the membrane can still hold the integrated configuration and there is no crack generated, suggesting their good flexibility.

The XRD analysis has been used to characterize the structure of the membranes. Fig. S1a shows that the as-prepared xerogel membrane is amorphous. After calcined at 500 °C for 2 h, obvious reflections at 25.3, 37.8, 48.0, 53.9, 55.0, and 62.7° indicate high-crystallinity anatase were formed (JCPDS, No. 21-1272). The FT-IR spectra (Fig. S1b) suggest the xerogel fibers contain a lot of organic groups, the existence of the absorption at 454 cm^{-1} reveals that the Ti-O-Ti has been formed before calcinations.

3.2. Effects of CeO_2 contents on the mechanical strength of the membrane

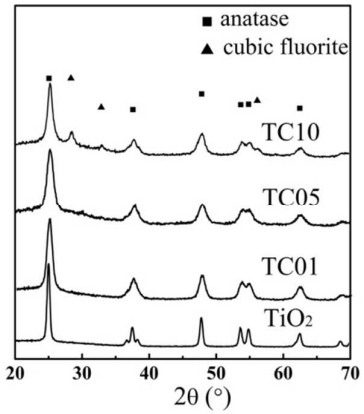

Fig. 2 XRD patterns of pure TiO_2 and TC01, TC05, TC10 samples.

The XRD patterns of the TiO_2 and CeO_2-doped TiO_2 samples with different Ti/Ce molar ratios (Fig. 2) show the characteristic peaks of anatase. For the TC01 sample, only diffraction peaks of anatase TiO_2 can be observed, which become broad comparing to pure TiO_2 fibrous membrane. Increasing the molar ratio of CeO_2:TiO_2 to 1:20

leads to further broadening of diffraction peaks. The peaks assigned to CeO_2 are not identified, mainly due to the small amount in the product. With the CeO_2 content increasing to 10%, the diffraction peaks of cubic fluorite CeO_2 appear. In addition, the average crystallite sizes of the CeO_2 doped TiO_2 nanofibers are calculated according to the (101) diffraction peaks of the anatase by the Scherrer's equation:

$$D = \frac{0.89\lambda}{\beta \cos\theta} \qquad (1)$$

where D is the average crystalline size, the λ is 0.1542 nm for the X-ray wavelength of CuKα radiation and β is full width at half-maxmum (fwhm) value for a particular 2θ angle. The calculated results based on the (101) plane of anatase were listed in Table 1. The CeO_2 doped TiO_2 nanofibers have relative smaller crystalline size (<10 nm) than the pure TiO_2 (17.3 nm). It reveals that the incorporation of CeO_2 can inhibit the grain growth of anatase. As reported, the radius of cerium ions (1.02 Å) is much bigger than that of titanium ions (0.68 Å). It is thus difficult for cerium to replace titanium in the crystal lattice.[40] As a result, the CeO_2 crystallizes between the TiO_2 nanocrystals (Fig. 3c), and the existence of the phase boundaries increases the diffusion distance of Ti atoms and inhibits the growth of TiO_2 nanocrystals.[41,42] The excessive CeO_2 will lead to the obvious growth of CeO_2 crystals, which can be seen from the HRTEM image (Fig. 3c). The growth of CeO_2 decreases the amount of phase boundaries, and the coarsening of the of TiO_2 nanocrystals occurs. The suitable molar ratio of CeO_2 in TiO_2 is very important. The SEM images of the TiO_2 nanofibers with different CeO_2 contents are presented in Fig. S2. The change trend of nanoparticles' size in the fibers coincides with that of the crystalline sizes from the XRD patterns.

The N_2 adsorption-desorption isotherms and corresponding pore size distribution of TiO_2 and CeO_2-doped TiO_2 samples are shown in Fig. S3. The isotherms presents a hysteresis loop in the relative pressure range of 0.4-0.9, indicating the presence of the inhomogeneous mesopores formed through the aggregation of the nanoparticles. The specific surface area by the Barrett-Emmett-Teller (BET) method is listed in Table 1. With the increase of the

amount of Ce, the specific surface area first increased and then decreased. The TC05 sample displays the largest specific surface area of 38.2 m^2 g^{-1} due to its smallest particle size. The BJH pore size distribution of all samples are in the range of 2-10 nm and a most probable pore size of about 3.7 nm. The mesopore structures of the samples can provide more reaction sites that are favorable for catalytic application.

Table 1. Effect of CeO_2 contents on the textural properties of the fibrous membranes.

Samples	Crystalline Phase	Crystalline Size (nm)	Surface Area S_{BET} (m^2/g)	Tensile Strength (MPa)
TiO_2	anatase	17.3	23.0	0.47
$Ce_{0.01}/TiO_2$	anatase	9.50	34.9	1.10
$Ce_{0.05}/TiO_2$	anatase	7.72	38.2	1.38
$Ce_{0.10}/TiO_2$	anatase+cerianite	9.86	35.2	0.60

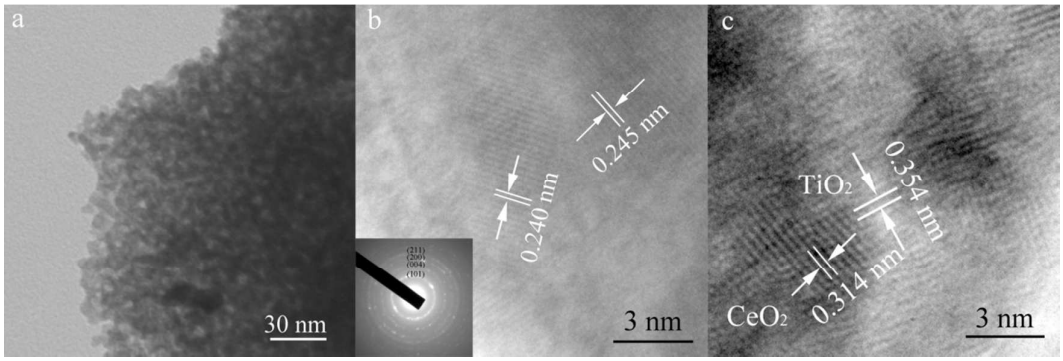

Fig. 3 HR-TEM images of TC05 (a, b) and TC10 (c). The inset is the corresponding SAED pattern.

The structural details of the CeO_2-TiO_2 samples are further analyzed by HR-TEM (Fig. 3). Nanoparticles with diameters of 7-10 nm can be identified from Fig. 3a, which are consistent with the corresponding XRD results described above. The HR-TEM image (Fig. 3b) displays the typical lattice fringes of *d*-spacing of *ca*.0.240 nm and 0.245 nm, which is in good agreement with the (004) and (103) planes of anatase. The selected area electron diffraction (SAED) pattern in the inset of Fig. 3b is made up of distinct diffraction rings, indicating polycrystalline anatase nature of the product. No information of Ce-dopant was obtained from the HR-TEM image of TC05 sample, and then the TC10 sample was further observed by HR-TEM technique. As shown in Fig. 3c, the interplanar spacing of 0.314 nm corresponds to the (111) lattice plane of CeO_2 and the spacing of 0.354 nm can be

ascribed to (101) plane of anatase TiO_2. The results indicate the CeO_2 crystallizes between TiO_2 nanoparticles, and their size increases with the content increasing, which are close with the change trends of XRD patterns in Fig. 2.

The X-ray energy dispersive spectroscopy (EDS) (Fig. S4a) exhibits the Ce and Ti signals and the atomic ratio of Ce to Ti are very close to the addition amounts in the preparation process of the sol. Bright-field SEM image of the TC05 sample and corresponding EDS elemental mapping are shown in Fig. S4b, which indicates Ce well disperses in the TiO_2 matrix.

Pd was introduced during the sol-gel process. The TEM image, SEM images, XRD patterns and optical image of Pd/TC05 are shown in Fig. S5. The Pd content in the fibers is too small to be detected. The same uniform diameters and smooth surface are observed. The high flexibility of membrane is also reserved. It reveals that the loading of Pd on the fibers hardly influences the essential structure of the membrane.

In order to confirm the chemical state of Pd in Pd/TC05, the sample was analyzed by XPS technique (Fig. S5f). The palladium displays two states in the fibers. Pd ($3d_{5/2,3/2}$) peaks at 335.4, 340.3 eV could be assigned to Pd^0 and the binding energy of the second Pd state (336.6 and 341.6 eV) belongs to Pd^{2+}.[43] Pd is present mostly in the Pd^0 state. Relative intensity of Pd($3d_{5/2}$) peak of Pd^{2+} and Pd^0 is 0.24. The result implies the actual state of Pd in the catalyst was in the form of metallic Pd and PdO. The content of palladium was semiquantitatively analyzed by XPS. The 0.32 atom% of Pd in the fibers is close to the added amount.

The application of the fibrous membrane in filtration mainly depends on the mechanical property and the spatial distribution of fibers. The mechanical properties of CeO_2-TiO_2 and Pd/CeO_2-TiO_2 membranes were studied by tensile testers. The strength of the membranes could be calculated by the following formula:

$$Tensile\ strength\ (MPa) = \frac{breaking\ force\ (cN)}{width\ (cm) \times thickness\ (\mu m)} \qquad (2)$$

The tensile strength-strain curves of composite membranes with different CeO_2 contents are shown in Fig. 4 and listed in Table 1. According to the results and discussion above, with the decrease of the crystalline size, the

tensile strength increases steadily. The strength of pure TiO_2 membrane is 0.47 MPa, while the incorporation of CeO_2 in TiO_2 nanofiber can markedly improve the mechanical property under the same heat treatment process. The TC05 sample exhibits a remarkable tensile stress of 1.38 MPa with an elongation at the break value of 1.3%, which is 3 times of pure TiO_2. The excessive CeO_2 in the fibers plays an opposite effect and the corresponding strength reduces to 0.60 MPa. After the Pd was loaded on the TC05 membrane, the tensile strength is 1.28 MPa and very close to that of TC05. The smaller crystalline sizes correspond to more grain boundary in the fibers, resulting in stress dispersion and strength enhancement of the fibers. The enhancement of the strength of the individual fibers can lead to the increase of the membrane's strength. According to previous reports, the present tensile stress is high enough for filtration application.[22]

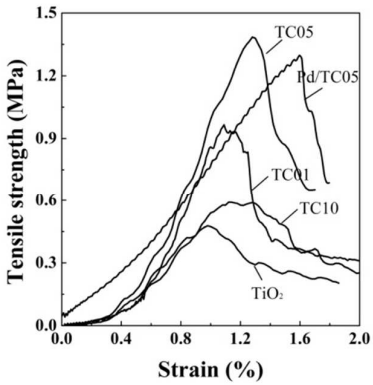

Fig. 4 The typical tensile strength-strain curves of TiO_2, CeO_2-TiO_2 and Pd/CeO_2-TiO_2 fibrous membranes.

3.3. Performance of fine air filtration and CO catalytic oxidation

The filtration performance of Pd/TC05 membranes was tested using charge neutralized NaCl aerosols in the size of 300-500 nm as filtering objects at a face velocity of 5.3 cm s^{-1}. The filtration efficiency and corresponding pressure drop were listed in Table 2. The different basis weights of the membranes can be obtained by adjusting the electrospinning time. The filtration efficiencies of the membranes with basis weights of 13.96, 14.87, 16.84, 18.45 and 20.76 g/m^2 were 96.46, 97.96, 99.86, 99.94 and 99.95%, respectively. Obviously, the filtration efficiency increases with the increase of basic weight. The corresponding pressure drops are 124, 140, 178, 230,

352 Pa. The results could satisfy the requirements of high efficiency particulate air filtration media.[22] In practical application, a good filter should possess a great filtration efficiency and a low pressure drop. The quality factor (QF) is a comprehensive parameter for comparing the filtration performance of filters.[44] The corresponding QF was listed in Table 2. The higher QF value means the better filtration performance. With the increase of the basis weight of the membrane, the QF value firstly increases and then decreases. The QF value indicates the membrane with the basic weight of 16.84 g m^{-2} has the best filtration performance. The suitable basic weight is necessary in practice, which can be easily controlled by adjusting the electrospinning time.

Table 2. Filtration performance *versus* the basis weights of CeO_2 doped TiO_2 fibrous membranes calcined at 500 °C under the air flow of 32 L min^{-1}.

Basic weight (g/m^2)	Filtration efficiency η (%)	Pressure drop △P (Pa)	Quality factor [a]
13.96	96.46	124	0.027
14.87	97.96	140	0.028
16.84	99.86	178	0.037
18.45	99.94	230	0.032
20.76	99.95	352	0.22

[a]: the quality factor (QF) is a comprehensive parameter for comparing filtration performance of different filters, which is defined as: $QF=[-\ln(1-\eta)]/\triangle P$, where η and △P represent the filtration efficiency and pressure drop, respectively.

In order to investigate the filtration performance of the membrane in a long term, a test for dust holding capacity was designed. Zirconia nanoparticles (density: 6.1 gm^{-3}) with the average size of 300 nm were adopted to replace the dust in the exhaust gas. The membrane with the basic weight of 18.45 g m^{-2} was chosen to compare the pressure drop before and after precipitate ZrO_2 particles on the membrane. The zirconia nanoparticles were dispersed in ethanol and filtrated from the fibrous membrane. After being dried at 60 °C for 24 h, the basic weight of 33.48 g m^{-2} was obtained. The corresponding pressure drop increased from 230 Pa to 340 Pa. If the dust density was adopted as 1.2 g m^{-3} and the dust level was 500 μg m^{-3}, the membrane could be used as long as 130 h under

the face velocity of 5.3 cm s^{-1}. The dust holding capacity is relative high compared with other filter and the membrane could be used for a long time.[45]

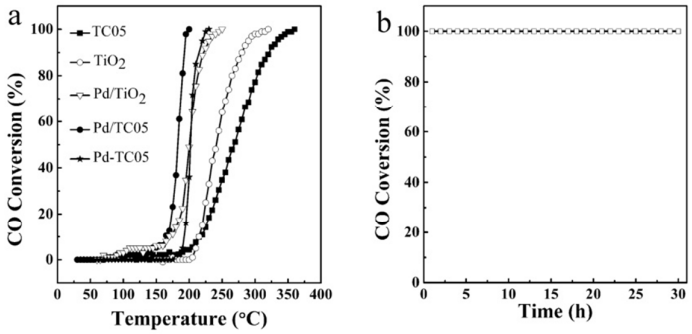

Fig. 5 Catalytic activities of the synthesized catalysts for CO conversion for TiO_2, TC05, Pd/TiO_2 and Pd/TC05 (a) and the catalytic stability of Pd/TC05 with the CO conversion of 100% over 30 h (b).

The catalytic activities for CO oxidation of pure TiO_2, TC05, Pd/TiO_2 and Pd/TC05 are shown in Fig. 5a. For comparison, the Pd-TC05 obtained by impregnating was also tested under the same condition. All samples exhibit catalytic ability toward CO oxidation. The temperature of CO conversion of 100% for pure TiO_2 (320 °C) is a little lower compared with the TC05 (360 °C) sample. Using CeO_2-TiO_2 or TiO_2 as catalyst, the oxide plays the dual functions of oxygen storage and catalysis. The catalytic property of the materials is closely related to their crystallinity,[46,47] which increases with the crystallinity increasing. In the present work, the doping of CeO_2 lowered the crystallinity of TiO_2, and then decreased the catalytic activity.

After Pd supported on the catalysts, the temperature of CO conversion shows an obvious decrease. Compared with Pd/TiO_2 (250 °C), Pd/CeO_2-TiO_2 shows the higher activity toward CO oxidation (200 °C). In addition, Pd/TC05 fibrous membrane also shows the better catalytic activity than Pd–TC05 by impregnating (225 °C). The loaded Pd by sol-gel process normally has the smaller size, which shows higher catalytic activity for CO oxidation. As for the Pd contained catalysts, the catalytic reaction occurs at a relative lower temperature. The oxides plays as the support to adsorb and store oxygen, and Pd acts as the catalyst to oxidize CO at a relative low temperature.[48,49]

Due to the addition of CeO_2, the oxygen storage ability of the product increases, which results in the enhancement of the catalytic ability.

The stability of catalytic activity of the Pd/TC05 fibrous membrane was tested under the conversion of 100% for 30 h. From Fig. 5b, the decrease of the catalytic activity does not be observed. The higher stability compared with other particulate catalysts[50] may be due to strong fixation of Pd in the fibers, which prevents the Pd nanoparticles from growing under high temperature, and the high activity of the membrane can be retained. The thermal stability of the membrane was also confirmed by the continuous calcination at 400 °C for 20 h. As shown in Fig. 6a, the membrane is still structural integrity with high flexibility. The SEM images (Fig. 6b) reveal the fibers still remain the original uniform diameters and smooth surface. The size of the nanoparticles that composed the fibers stays the same. The results are also verified by the XRD pattern (Fig. 6c), from which the changes of diffraction peaks are indecipherable, indicating that the sample keeps the crystal structure of anatase without any other impurities. The tensile strength of the fibrous membrane after treatment can be up to 1.22 MPa (Fig. 6d), almost the same as the initial value (1.28 MPa).

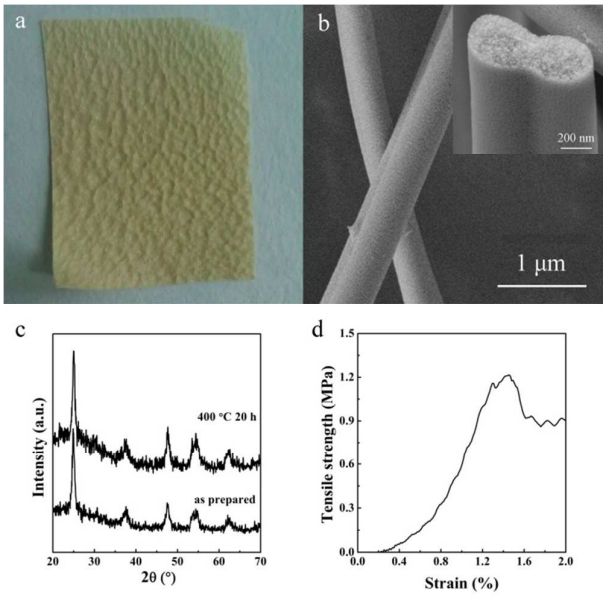

Fig. 6 Optical image (a), SEM images (b), XRD patterns (c), and tensile stress-strain curve (d) of the Pd/TC05

fibrous membrane calcined at 400 °C for 20 h.

The catalytic performance and stability clearly suggest that the fibrous membrane can meet the demands of practical application under the rigid conditions for a long time. For example, it is necessary for the metallurgy industry to remove the dust at a relatively high temperature.[22] Thus, the high stability is suitable for the practical application. Those results confirm that the combination of CO catalytic oxidation with fine air filtration is feasible.

4. Conclusions

In this paper, the flexible CeO_2-TiO_2 fibrous membrane was prepared for the first time with the tensile strength up to 1.38 MPa. The size decreasing of the particles in the fibers upon the introducing CeO_2 increased the grain boundaries, and then the mechanical strength of the fibers and the membranes significantly enhanced. The noble metal can be loaded on the fibers *via* the sol-gel process and do little influence on the strength of the membrane. The Pd/CeO_2-TiO_2 fibrous membrane exhibits good filtration performance with the filtration efficiency of 99.86% and the pressure drop of 178 Pa. Besides, the fibrous membrane shows favorable catalytic property and excellent catalytic stability toward CO oxidation. The excellent properties could satisfy the rigid demands of the practical operation and make the filtration media multifunctional to become a reality. This work opens up the views of the new applied field of flexible inorganic fibrous membranes.

Acknowledgements

This work is supported by the Key Projects in the Science & Technology Pillar Program of China (No. 2013BAC01B02) and the National High Technology Research and Development Program of China (No. 2012AA03A210).

References

1 International Agency for Research on Cancer, 2013, http://www.iarc.fr/en/media-centre/iarcnews/pdf/pr221_E.pdf.

2 T. Lancet, *The Lancet*, 2014, **383**, 845.

3 N. Künzli, R. Kaiser, S. Medina, M. Studnicka, O. Chanel, P. Filliger, M. Herry, F. Horak, V. Puybonnieux-Texier, P. Quénel, J. Schneider, R. Seethaler, J.C. Vergnaud and H. Sommer, *The Lancet*, 2000, **356**, 795.

4 C. K. Chan and X. Yao, *Atmos. Environ.*, 2008, **42**, 1.

5 B. R. T. Simoneit, *Appli.Geochem.*, 2002, **17**, 129.

6 M. Wilhelm and B. Ritz, *Environ. Health Perspect.*, 2005, **113**, 1212.

7 D. Gorman, A. Drewry, Y. L. Huang and C. Sames, *Toxicology*, 2003, **187**, 25.

8 A. G. Chmielewski, J. Licki, A. Pawelec, B. Tymiński and Z. Zimek, *Radiat. Phys. Chem.*, 2004, **71**, 441.

9 A. D. Shepelev and V. A. Rykunov, *J. Aerosol Sci.*, 1995, 919-920.

10 R. Barhate and S. Ramakrishna, *J. Membr.Sci.*, 2007, **296**, 1.

11 V. Thavasi, G. Singh and S. Ramakrishna, *Energy Environ. Sci.*, 2008, **1**, 205.

12 Z. M. Huang, Y. Z. Zhang, M. Kotaki and S. Ramakrishna, *Compos. Sci. Technol.*, 2003, **63**, 2223.

13 D. Li and Y. Xia, *Adv. Mater.*, 2004, **16**, 1151.

14 A. Greiner and J. H. Wendorff, *Angew.Chem. Int. Ed.*, 2007, **46**, 5670.

15 K. Yoon, K. Kim, X. Wang, D. Fang, B. S. Hsiao and B. Chu, *Polymer*, 2006, **47**, 2434.

16 K. Yoon, B. S. Hsiao and B. Chu, *J. Mater. Chem.*, 2008, **18**, 5326-5334.

17 R. Gopal, S. Kaur, Z. Ma, C. Chan, S. Ramakrishna and T. Matsuura, *J. Membr. Sci.*, 2006, **281**, 581.

18 M. Guo, B. Ding, X. Li, X. Wang, J. Yu and M. Wang, *J. Phys. Chem. C*, 2009, **114**, 916.

19 R. Ramaseshan, S. Sundarrajan, R. Jose and S. Ramakrishna, *J. Appl. Phys.*, 2007, **102**, 111101.

20 Y. E. Mao, R. Wang, D. Chen, Z. Liu and T. Liu, *ACS Appl. Mater. Interfaces*, 2012, **4**, 5353.

21 X. Mao, Y. Si, Y. Chen, L. Yang, F. Zhao, B. Ding and J. Yu, *RSC Adv.*, 2012, **32**, 12216.

22 Y. Wang, W. Li, Y. Xia, X. Jiao and D. Chen, *J. Mater. Chem. A*, 2014, **2**, 15124.

23 M. Haruta and M. Daté, *Appl.Catal. A*, 2001, **222**, 427.

24 N. Li, Q. Y. Chen, L. F. Luo, W. X. Huang, M. F. Luo, G. S. Hu and J. Q. Lu, *Appl.Catal. B,* 2013, **142–143**, 523.

25 X. S. Huang, H. Sun, L. C. Wang, Y. M. Liu, K. N. Fan and Y. Cao, *Appl. Catal. B,* , 2009, **90**, 224.

26 K. An, S. Alayoglu, N. Musselwhite, S. Plamthottam, G. Melaet, A. E. Lindeman and G. A. Somorjai, *J. Am. Chem. Soc.*, 2013, **135**, 16689.

27 M. Nishibori, W. Shin, N. Izu, T. Itoh and I. Matsubara, *Catal. Today*, 2013, **201**, 85.

28 J. A. Wang, L. F. Chen, M. A. Valenzuela, A. Montoya, J. Salmones and P. D. Angel, *Appl. Surf. Sci.*, 2004, **230**, 34.

29 X. Wang, J. S. Tian, Y. H. Zheng, X. L. Xu, W. M. Liu and X. Z. Fang, *ChemCatChem*, 2014, **6**, 1604.

30 I. D. González, R. M. Navarro, W. Wen, N. Marinkovic, J. A. Rodriguéz, F. Rosa and J. L. G. Fierro, *Catal. Today*, 2010, **149**, 372.

31 H. Zhu, Z. Qin, W. Shan, W. Shen and J. Wang, *J.Catal.*, 2005, **233**, 41.

32 V. Idakiev, T. Tabakova, K. Tenchev, Z.-Y. Yuan, T.-Z. Ren and B.-L. Su, *Catal. Today*, 2007, **128**, 223.

33 H. Zhu, Z. Qin, W. Shan, W. Shen and J. Wang, *J. Catal.*, 2004, **225**, 267.

34 D. A. H. Hanaor and C. C. Sorrell, *J. Mater. Sci*, 2011, **46**, 855.

35 K. Huang, X. Chu, W. Feng, C. Zhou, W. Si, X. Wu, L. Yuan and S. Feng, *Chem. Eng. J.*, 2014, **244**, 27.

36 S. Xu, D. Sun, H. Liu, X. Wang and X. Yan, *Catal. Comm.*, 2011, **12**, 514.

37 T. Cao, Y. Li, C. Wang, L. Wei, C. Shao and Y. Liu, *J. Sol-Gel Sci. Technol*, 2010, **55**, 105.

38 C. J. Li, B. Wang and J. N. Wang, *J. Nanosci. and Nanotechnol.*, 2012, **12**, 2522.

39 T. Cao, Y. Li, L. Wei, C. Shao, Y. Liu and C. Wang, *Mater. Res. Bull.*, 2010, **45**, 1406.

40 G. Xiao, X. Huang, X. Liao and B. Shi, *J. Phys. Chem. C*, 2013, **117**, 9739.

41 B. M. Reddy, A. Khan, and P. Lakshmanan, *J. Phys. Chem. B,* 2005, **109**, 3355.

42 N. Aman, P. K. Satapathy, T. Mishra, M. Mahato and N. N. Das, *Mater. Res. Bull.*, 2011, **47**, 179.

43 K. R. Priolkar, P. Bera, P. R. Sarode, M. S. Hegde, S. Emura, R. Kumashiro and N. P. Lalla, *Chem. Mater.,* 2002, **14**, 2120.

44 G. Viswanathan, D. B. Kane and P. J. Lipowicz, *Adv. Mater.*, 2004, **16**, 2045.

45 C. Tekmen, 31st Annual Technology Meeting on Air Cleaning and Contamination Control, At waseda, Tokyo, 2014, http://www.researchgate.net/publication/262792664.

46 T. Tabakova, V. Idakiev, D. Andreeva and I. Mitov, *Appl.Catal. A*, 2000, **202**, 91.

47 G. Glaspell, H. M. Hassan, A. Elzatahry, L. Fuoco, N. R. Radwan and M. S. El-Shall, *J. Phys. Chem. B*, 2006, **110**, 21387.

48 A. A. Shutilov, G. A. Zenkovets, I. Y. Pakharukov and I. P. Prosvirin, *Kinet.Catal.*, 2014, **55**, 111.

49 A. Satsuma, M. Yanagihara, K. Osaki, Y. Saeki, H. Liu, Y. Yamamoto, S. Arai and J. Ohyama, *RSC Adv.*, 2014, **4**, 54187.

50 G. Dong, J. Wang, Y. Gao and S. Chen, *Catal. Lett.*, 1999, **58**, 37.

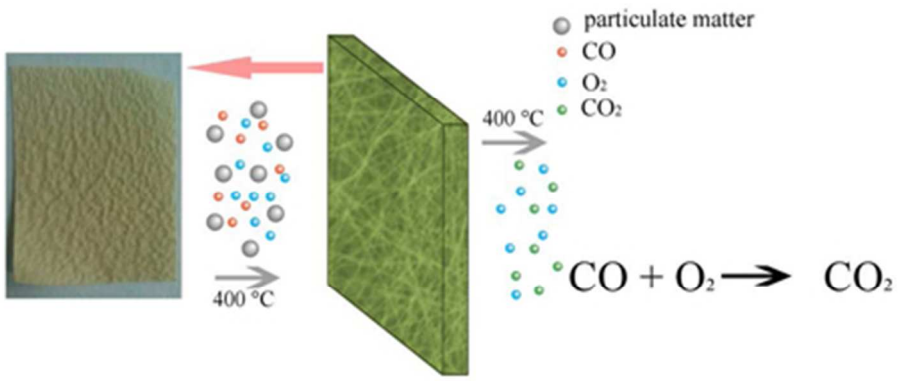

129x50mm (96 x 96 DPI)